Lv *et al. EURASIP Journal on Advances in Signal Processing* (2019) 2019:4
https://doi.org/s13634-018-0599-8

EURASIP Journal on Advances in Signal Processing

RESEARCH Open Access

Energy-efficient multi-cell resource allocation in cognitive radio-enabled 5G systems

Hengwei Lv, Pandong Li, Qinmengying Yan and Haijian Zhang*

Abstract

In this paper, we propose an energy-efficient resource allocation (RA) algorithm in cognitive radio-enabled 5th generation (5G) systems, where the scenario including one primary system and multiple secondary cells is considered. Because of the high spectrum leakage of traditional orthogonal frequency division multiplexing (OFDM), alternative modulation schemes regarded as the potential air interfaces in 5G are analyzed, e.g., filter bank-based multi-carrier (FBMC), generalized frequency division multiplexing (GFDM), and universal filtered multi-carrier (UFMC). Our objective is to maximize the whole energy efficiency of secondary system defined by the ratio of the capacity to the total power consumption subject to some practical constraints. The general formulation leads to a non-convex mixed-integer nonlinear programming problem with fractional structure, which is challenging to solve due to its intractability and significant complexity. Therefore, we resort to an alternate optimization framework to optimize the variables of subcarrier assignment and power allocation, where successive convex approximation (SCA) is employed so that the general formulation is finally transformed into a solvable convex problem. Numerical results validate the effectiveness of the proposed RA algorithm, and the comparison with some existing RA algorithms is conducted. In addition, the performance of using different 5G candidate waveforms in the energy-efficient RA algorithm is also presented and discussed.

Keywords: 5G, Cognitive radio, Modulation schemes, Energy efficiency, Resource allocation

1 Introduction

With the explosive growth of various communication services, more and more mobile terminals or users are seeking for accessing the communication networks. However, the current 4th generation (4G) communication technologies cannot meet the increasing communication demand, which greatly drives the development of the 5th generation (5G) communication technologies [1–3]. It has been expected that 5G not only should satisfy the great communication needs but the efficient utilization of scarce spectral resource should be also ensured. On the one hand, the current policy of the exclusive spectrum allocation cannot maintain the supply of additional spectrum to accommodate more mobile users, support higher capacity and lower latency requirements, and provide ubiquitous connectivity of the Internet of Things. On the other hand, the inadequate spectrum resource is not efficiently utilized, and a large portion of the spectrum is idle without being accessed by licensed systems [4, 5].

As a result, the concept of cognitive radio (CR) is put forward to solve the problem of 5G spectrum scarcity and improve the spectral efficiency by allowing secondary users (SUs) to occupy the idle spectrum [6, 7]. The CR-enabled 5G systems provide the possibility that SUs can autonomously access the most meritorious spectrum and gain higher network capacity [8]. Currently, how to efficiently allocate spectrum resource to SUs becomes one of the key research topics in 5G. Existing resource allocation (RA) works aim at either maximizing the system capacity or minimizing the energy consumption. The large number of users and diverse services in 5G signify the huge system consumption; thus, maximizing the energy efficiency plays a critical role of performance assessment in future communications [9–11]. This paper takes the

*Correspondence: haijian.zhang@whu.edu.cn
Signal Processing Laboratory, School of Electronic Information, Wuhan University, Bayi Road, Wuhan 430072, People's Republic of China

system consumption into account, and focuses on the energy-efficient multi-cell RA algorithm in CR-enabled 5G systems.

1.1 Related work

In the literature, plenty of existent works pay attentions to the RA problem by assuming one primary cell and a single secondary cell. The authors in [12] utilized the spectrum holes in primary user (PU) bands as well as active PU bands to propose a low complexity suboptimal solution for orthogonal frequency division multiplexing (OFDM) and filter bank-based multi-carrier (FBMC) systems. Spectrum sensing and resource allocation were jointly considered in [13], and the water filling algorithm is modified for the optimization problem. In [14], the authors proposed an algorithm to maximize the system capacity through exploiting the problem structure to speed up the convergence. The authors in [15] investigated the effective capacity maximization problem under statistical delay guarantee by the Lagrangian dual decomposition method. An energy consumption issue with channel uncertainty was studied in [16], and a fast algorithm is derived to settle the quasi-convex problem. In [17], the resource allocation problem was solved by the Hungarian algorithm and the gradient projection method. However, it is noteworthy that the above RA algorithms may be not suitable for handling more complicated situations where multiple secondary cells are involved, which is the practical scenario in future ultra-dense 5G networks.

It is quite difficult to solve the CR RA problem of multi-cell due to the complicated system structure and the existence of co-channel interference between different cells. To make this problem tractable, some RA algorithms have been developed. A distributed algorithm containing two loops [18] was designed for the weighted sum-rate maximization problem with multi-cell uplink-downlink throughput. An interference-limited method was presented in [19], where the co-channel interference is assumed to be constant and then transformed into a constraint. In [20, 21], the non-cooperative game theory was adopted to solve the problem of multi-cell, and Nash equilibrium is guaranteed. However, less efforts have been devoted to the research of the energy-efficient multi-cell resource allocation. An iterative subchannel allocation and power allocation algorithm was proposed in [22] for joint optimization of energy and spectral efficiency. In [23], a distributed resource allocation scheme-based game theory, taking user fairness and priority into consideration, was proposed to solve the energy-efficient RA problem. The problem of power control jointly considering energy efficiency and delay was solved in [24] by non-cooperative game. The energy-efficient downlink resource allocation in heterogeneous networks was investigated in [25], where a non-concave nonlinear objective function and nonlinear constraints are incorporated. Fractional programming and branch-and-bound method are utilized to obtain the solution. The authors in [26] considered an equivalent non-fractional form of the formulated problem and proposed an iterative algorithm to optimize the objective. Nevertheless, the aforementioned literatures did not investigate the impact of spectral leakage of different 5G waveforms on energy efficiency.

1.2 Contributions

In this paper, we propose an energy-efficient RA algorithm for the scenario including one primary cell and multiple secondary cells. We try to maximize the energy efficiency of all the secondary cells subject to some practical constraints. Although the constructed expression belongs to a mixed-integer nonlinear programming with high computation complexity, it can be well solved by the proposed RA algorithm. Compared to the existing works, the contributions of the proposed RA algorithm are as follows:

- A practical energy-efficient multi-cell RA problem in CR-enabled 5G systems is formulated. In practice, the interference between the primary system and the secondary cells actually exists due to the spectral leakage; thus, the interference vectors in [27–30] are employed in the proposed RA formulation. To the best of our knowledge, there are few works which consider the quantified interference vectors to formulate the objective function and its corresponding constraints in 5G resource allocation problem.
- The general formulation is a mixed-integer nonlinear programming problem, and we propose an efficient RA algorithm to transform the intractable non-convex problem into a convex one. Specifically, the variables of subcarrier assignment and power allocation are alternately optimized. Once given the subcarrier assignment, a novel transformation is utilized to eliminate the fractional structure and successive convex approximation (SCA) is adopted to solve the power allocation. Moreover, the convergent property can be ensured. The proposed RA algorithm is compared with some existing algorithms, and the simulation results show the advantages of the proposed algorithm.
- The impacts of spectral leakage by using different multi-carrier modulation schemes on energy efficiency are quantitatively analyzed. Although OFDM has been widely used in many applications, e.g., long-term evolution (LTE), it can hardly satisfy the need of supporting asynchronous transmission to avoid the heavy synchronization signaling overhead caused by massive terminals [31]. Moreover, the

significant spectral leakage of OFDM will induce severe adjacent channel interference. In 5G networks, more flexible 5G waveforms [32] are required to overcome the upcoming challenges, e.g., FBMC [33–35], generalized frequency division multiplexing (GFDM) [36], and universal filtered multi-carrier (UFMC) [37]. Most of the existing RA algorithms only take either OFDM [14–16] or OFDM/FBMC [12, 20, 38] into account, and it still needs to make a thorough inquiry of the specific influence about different waveforms. In our RA algorithm, all of the above 5G waveforms are compared by evaluating the effect of waveforms on energy efficiency, and the results can provide a reference base for designing and selecting the physical waveform in 5G systems.

The remainder of this paper is organized as follows. In Section 2, the system model is illustrated and the optimization problem is formulated. Section 3 describes the optimization frame of the proposed resource allocation algorithm. The complexity of the proposed algorithm is analyzed in Section 4. The simulation results are presented in Section 5. Finally, we conclude the paper in Section 6.

2 System model and problem formulation

2.1 System model

In the context of CR-enabled 5G systems, we assume a system scenario where a primary system and multiple secondary cells coexist, as illustrated in Fig. 1. The primary system is located in the center of the whole system, and it is comprised of a primary base station (PBS) and PUs. While the secondary CR system consists of multiple secondary cells, the secondary cells are uniformly distributed around the primary system. Let $\mathcal{N} = \{1, 2, ..., n, ..., N\}$ denote the set of secondary cells, and in the n_{th} cell, there is a secondary base station (SBS) serving M SUs denoted by $\mathcal{M}_n = \{1_n, 2_n, ..., m_n, ..., M_n\}$.

Given the above system model, we make some assumptions as below:

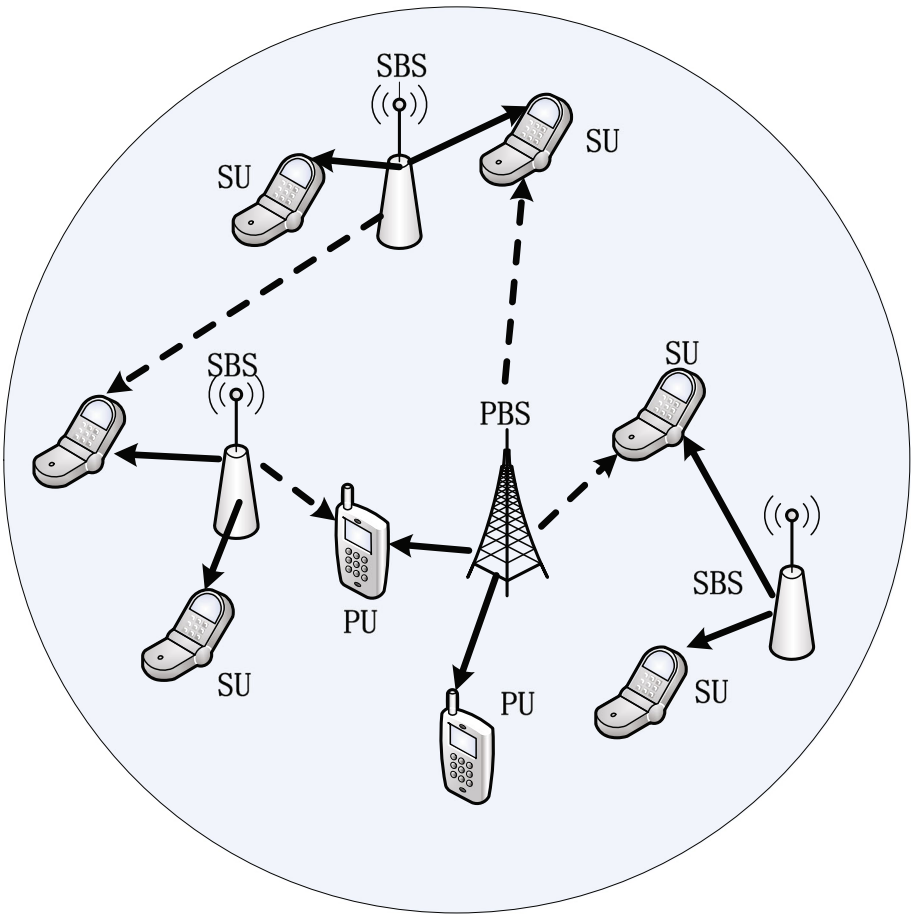

Fig. 1 System model. CR-enabled 5G system model containing one primary system and multiple secondary cells (The solid arrow lines denote the communication links and the dashed arrow lines denote the interference links, which include the interferences among secondary cells, secondary cells to the primary system and vice verse)

- Considering the downlink transmission, each user receives signals from their own base station respectively, and the signals from other base stations are regarded as interference, i.e., each user is only attached to one cell [38].
- Assuming that SUs are randomly located around their own SBS, all base stations serve as accessing points to their corresponding users, and single antenna is equipped for the transmitter and receiver [20].
- It is practical to assume that the primary system and all the secondary cells are asynchronized; thus, the interference due to spectral leakage exists between primary and secondary systems [27].
- All the secondary cells are synchronized, and the spectrum sensing is assumed to be achieved by a public sensing node. The sensing results are transmitted to the SBSs by a common control channel, i.e., all secondary cells share the same sensing results.
- Since the secondary cells and primary cell are subordinate to two different systems, generally, their cross-gains are unaccessible. But for simplicity and providing an interference protection to primary cell, we only estimate the channel gains from secondary system to primary cell.

After receiving the sensing results, the SBS allocates the available frequency resource to its attached SUs. The sketch map of possible sensing results is depicted in Fig. 2. The whole frequency band is divided into some subcarriers, where the set of available and occupied subcarriers is denoted as $\mathcal{F} = \{1, \ldots, f, \ldots, F\}$ and $\mathcal{L} = \{1, \ldots, l, \ldots, L\}$, respectively. The index difference between the f_{th} available subcarrier and the l_{th} unavailable subcarrier is $\pi(f, l) = \left|\mathcal{F}_{(f)} - \mathcal{L}_{(l)}\right|$. Denote the power on the f_{th} available subcarrier accessed by the m_{th} SU of the n_{th} cell as p^{nf}, and the channel gain from the n_{th} SBS to the m_{th} SU is denoted as g_{nm}^{nf}. Therefore, the corresponding signal to interference plus noise ratio (SINR) is expressed as:

$$\ell_m^{nf} = \frac{p^{nf} g_{nm}^{nf}}{\sigma^2 + I_{\text{ps}} + I_{\text{ss}}}, \tag{1}$$

where σ^2 means additive white Gaussian noise power, I_{ps} denotes the interference from primary system which is induced by the asynchronization transmission, and I_{ss} denotes co-channel interference between secondary cells. The power variable p^{nf} is gathered into the matrix $\boldsymbol{P}$ with size $N \times F$.

According to the aforementioned assumptions, the asynchronous interference only exists between the primary and secondary systems. In order to compute the interference I_{ps}, we resort to the interference vector model for quantifying the asynchronization transmission interference between primary and secondary systems. The interference vectors of different candidate waveforms in 5G are shown in Table 1, where the value of the cases of perfect synchronization (PS), OFDM, and FBMC is cited from [27] while the value of the cases of UFMC and GFDM is cited from [30]. Supposing that a single complex symbol is transmitted with unit power and unit channel gain in a subcarrier, each element of one interference vector corresponds to the quantity of the out of band radiation, i.e., V means the spilled power from the interferer subcarrier with unit power and unit channel gain to the victim subcarrier. And the quantities of interference less than 10^{-3} are all ignored. It is noted in Table 1 that each subcarrier will introduce interference to its eight adjacent subcarriers for OFDM (if the spectral distance is larger than 8, the interference will be less than 10^{-3} and ignored), and the first adjacent subcarrier suffers from the severest interference with amount of $8.94\text{E} - 2$. For the

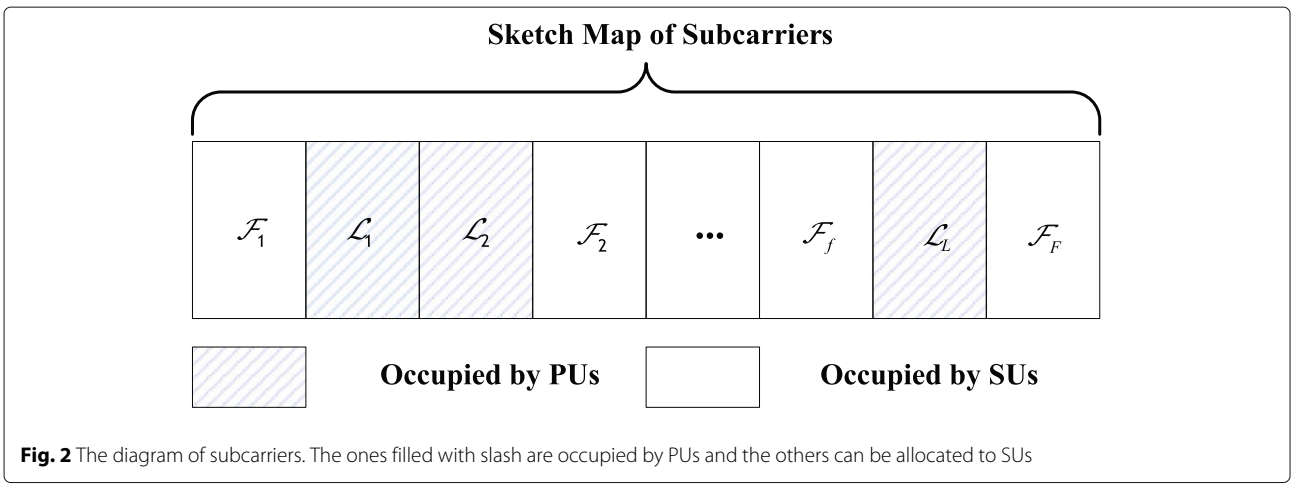

Fig. 2 The diagram of subcarriers. The ones filled with slash are occupied by PUs and the others can be allocated to SUs

Table 1 Interference vector table of different candidate waveforms in 5G

	$\pi(f,l)=1$	$\pi(f,l)=2$	$\pi(f,l)=3$	$\pi(f,l)=4$	$\pi(f,l)=5$	$\pi(f,l)=6$	$\pi(f,l)=7$	$\pi(f,l)=8$
V_{PS}	0	0	0	0	0	0	0	0
V_{OFDM}	8.94E − 2	2.23E − 2	0.995E − 2	0.560E − 2	0.359E − 2	0.250E − 2	0.184E − 2	0.112E − 2
V_{FBMC}	8.81E − 2	0	0	0	0	0	0	0
V_{UFMC}	12.27E − 2	0	0	0	0	0	0	0
V_{GFDM}	4.80E − 2	4.18E − 2	0.140E − 2	0	0	0	0	0

case of FBMC, it can be seen that the number of subcarriers interfered due to spectral leakage is 1. Intuitively, FBMC can achieve better interference protection to primary system due to its slight spectral leakage compared to OFDM. The analogous conclusion can be drawn for the cases of UFMC and GFDM.

Consequently, the interferences of I_{ps} and I_{ss} can be respectively defined as follows:

$$I_{\mathrm{ps}} = \sum_{l=1}^{L} P_p^l h_{\mathrm{ps}}^{nmf} V_{\pi(f,l)}, \tag{2}$$

$$I_{\mathrm{ss}} = \sum_{n'\in\mathcal{N}, n'\neq n}^{N} p^{n'f} g_{nm}^{n'f}, \tag{3}$$

where P_p^l denotes the power on the l_{th} subcarrier occupied by PU, h_{ps}^{nmf} denotes the channel gain from PBS to the m_{th} SU of the n_{th} cell on the f_{th} available subcarrier, and $g_{\mathrm{nm}}^{n'f}$ denotes the channel gain from the n'_{th} SBS to the m_{th} SU of the n_{th} cell on the f_{th} available subcarrier.

2.2 Problem formulation

According to Shannon capacity formula, the sum capacity of all SUs is formulated as:

$$\sum_{n=1}^{N}\sum_{m=1}^{M}\sum_{f=1}^{F}\theta_f^{nm}\log_2\left(1+\ell_m^{nf}\right), \tag{4}$$

where θ_f^{nm} denotes the indicator of subcarrier assignment, i.e., $\theta_f^{nm}=1$ means the f_{th} available subcarrier is allocated to the m_{th} SU of the n_{th} cell, otherwise $\theta_f^{nm}=0$. Define $\boldsymbol{\theta}$ as the set of θ_f^{nm}. As discussed earlier, the system objective of this paper is to improve the energy efficiency; therefore, we aim to maximize the ratio of the sum capacity to the sum power consumption as below:

$$\frac{\sum_{n=1}^{N}\sum_{m=1}^{M}\sum_{f=1}^{F}\theta_f^{nm}\log_2\left(1+\ell_m^{nf}\right)}{\sum_{n=1}^{N}\left(P_{\mathrm{dp}}+P_{\mathrm{sp}}+\sum_{f=1}^{F}\xi p^{nf}\right)}, \tag{5}$$

where the first term P_{dp} in the denominator denotes the dynamic power consumption, e.g., power radiation of circuit blocks in radio frequency chain, while the second term P_{sp} is the static power employed for cooling system and power supply, and ξ in the last term means the inverse of power amplifier efficiency [39, 40].

In wireless communication networks, the optimization problem of resource allocation generally involves some constraints. Some practical constraints considered in this work are listed as follows:

$$\sum_{f=1}^{F} p^{nf} \le P_{\mathrm{th}}, \quad \forall n; \tag{6a}$$

$$0 \le p^{nf} \le P_{\mathrm{sub}}, \quad \forall n,f; \tag{6b}$$

$$\theta_f^{nm} \in \{0,1\}, \quad \forall n,m,f; \tag{6c}$$

$$\sum_{m=1}^{M} \theta_f^{nm} = 1, \quad \forall n,f. \tag{6d}$$

The constraint (6a) is the sum power budget of each secondary cell, where the sum power of all available subcarriers in each cell should be no more than P_{th}. The constraint (6b) limits the power level on each subcarrier, which should not exceed P_{sub}. The last two constraints (6c) and (6d) indicate that each subcarrier must be accessed at most one user at a given time.

As a CR-enabled 5G system, the constraint keeping the interference from secondary cells to primary system must be considered. Denote h_{sp}^{nf} as the real channel gain from the n_{th} SBS to PU on the f_{th} available subcarrier. According to the last item in the assumptions, h_{sp}^{nf} is unknown and needs to be estimated.

The works in [41, 42] give a real propagation model of the channel, which decomposes h_{sp}^{nf} into L_{sp}^{nf} for large scale fading and S_{sp}^{nf} for small scale fading respectively, i.e., $h_{\mathrm{sp}}^{nf} = L_{\mathrm{sp}}^{nf} S_{\mathrm{sp}}^{nf}$. The L_{sp}^{nf} is only decided by shadowing and distance between the communicating parties. The S_{sp}^{nf} can be described as the product of two conjugate circular symmetric complex Gaussian variables with zero mean and unit variance. Thus S_{sp}^{nf} has a Gamma distribution with unit shape parameter and unit scale parameter, i.e., $S_{\mathrm{sp}}^{nf} \sim \Gamma(1,1)$.

By introducing a channel estimated margin S_{mar}, we can use $\widetilde{h}_{\mathrm{sp}}^{nf} = L_{\mathrm{sp}}^{nf}(1+S_{\mathrm{mar}})$ as the estimation of h_{sp}^{nf}. Define

the case if h_{sp}^{nf} is larger than $\widetilde{h}_{\mathrm{sp}}^{nf}$ as the outage. The outage probability can be represented as:

$$P_{\mathrm{out}} = \mathrm{Pro}\left(h_{\mathrm{sp}}^{nf} > \widetilde{h}_{\mathrm{sp}}^{nf}\right) = \mathrm{Pro}\left(S_{\mathrm{sp}}^{nf} > (1 + S_{\mathrm{mar}})\right). \tag{7}$$

The cumulative distribution function of S_{sp}^{nf} is the regularized Gamma function, and Eq. (7) can be further formulated as:

$$1 - P_{\mathrm{out}} = \frac{\gamma(1, 1 + S_{\mathrm{mar}})}{\Gamma(1)}, \tag{8}$$

where $\gamma(\cdot)$ is the lower incomplete Gamma function. For a given outage probability P_{out}, we have:

$$S_{\mathrm{mar}} = \log_e\left(\frac{1}{P_{\mathrm{out}}}\right) - 1. \tag{9}$$

Through the prescribed P_{out}, the estimated channel gain $\widetilde{h}_{\mathrm{sp}}^{nf}$ can be obtained. The critical interference constraint can be formulated as:

$$\sum_{f=1}^{F} p^{nf} \widetilde{h}_{\mathrm{sp}}^{nf} V_{\pi(f,l)} \le I_{\mathrm{th}}^{l}, \quad \forall n, l, \tag{10}$$

where I_{th}^{l} in (10) is the interference threshold and prescribed by the guarantee coefficient β of PU capacity, which is defined as:

$$\log_2\left(1 + \frac{P_{p}^{l} g_{\mathrm{pp}}^{l}}{\sigma^2 + I_{\mathrm{th}}^{l}}\right) = \beta \log_2\left(1 + \frac{P_{p}^{l} g_{\mathrm{pp}}^{l}}{\sigma^2}\right), \tag{11}$$

where g_{pp}^{l} is the channel gain from PBS to the PU occupying the l_{th} unavailable subcarrier. The larger the value of β is, the lower the interference threshold is.

Based on the abovementioned analysis, we express the optimization problem as **Q1**:

$$\max_{p^{nf}, \theta_f^{nm}} \frac{\sum_{n=1}^{N}\sum_{m=1}^{M}\sum_{f=1}^{F} \theta_f^{nm} \log_2\left(1 + \ell_m^{nf}\right)}{\sum_{n=1}^{N}\left(P_{\mathrm{dp}} + P_{\mathrm{sp}} + \sum_{f=1}^{F} \xi p^{nf}\right)}, \quad \text{s.t. (6a)} \sim \text{(6d)}, \text{(10)}. \tag{12}$$

3 Optimization method via alternate way

It is noted that **Q1** in (12) is a mixed-integer nonlinear programming problem, which is quite difficult to solve. Firstly, the integer indicator variable θ_f^{nm} equals to 1 or 0, and the real variable p^{nf} is involved. Both discrete and continuous variables will give rise to high complexity. Secondly, the ratio of a non-convex function to a linear function in (5) is also a non-convex structure. Finally, the co-channel interference might also induce the non-convex property. In this section, an efficient optimization scheme based on alternate optimization and SCA is proposed to transform **Q1** into a solvable problem, and for a clear illustration, it is summarized in Algorithm 1, which includes the procedures of subcarrier assignment and power allocation. In the following, these two parts will be described in details.

Algorithm 1 Proposed algorithm based on alternate optimization and SCA

Initialization: Set $t_1 = 0$, initialize $\mathbf{P}_{t_1}$ with a feasible power, ϵ_1;

1: **repeat**
2: $t_1 = t_1 + 1$;
3: Updating $\boldsymbol{\theta}_{t_1}$ according to (13)
4: Set $t_2 = 0$, initialize $\left\{\widetilde{\mathbf{P}}_{t_2}, \widetilde{x}_{t_2}, \widetilde{y}_{t_2}\right\}$ and ϵ_2
5: **repeat**
6: $t_2 = t_2 + 1$;
7: Approximate the constraints (15d) and (15e) according to (16) and (20);
8: Use CVX to solve **P4** and obtain $\left\{\mathbf{P}', x, y\right\}$;
9: Set $\widetilde{\mathbf{P}}_{t_2} = \exp\left(\mathbf{P}'\right), \widetilde{x}_{t_2} = x, \widetilde{y}_{t_2} = y$;
10: **until** $\left\|x_{t_2+1} - x_{t_2}\right\| \le \epsilon_2$
11: Set $\mathbf{P}_{t_1} = \widetilde{\mathbf{P}}_{t_2}$
12: **until** $\left\|\mathbf{P}_{t_1+1} - \mathbf{P}_{t_1}\right\| \le \epsilon_1$

Output: $\boldsymbol{\theta}, \boldsymbol{P}$

3.1 Heuristic subcarrier assignment

In order to solve the optimization problem **Q1**, the subcarrier assignment indicator θ_f^{nm} should be firstly excluded from the objective function and constraints. Because the problem **Q1** will generate M^{NF} possible subcarrier allocation schemes, which is prohibitively expensive especially in a high-dimensional system. To avoid the unbearable complexity, a heuristic subcarrier assignment is employed by means of an alternate manner.

For a given power allocation, the problem **Q1** is equivalent to maximizing the total system capacity subject to the constraints (6c) and (6d). Generally, it is not sufficient to assign subcarriers to one user with the best channel gain. In this context, the co-channel interference and the power on subcarriers are not taken into account. To realize the maximal capacity of communication networks, subcarriers can be allocated by employing the maximal SINR criterion [43]. In our work, we assume an initial feasible power distribution is given[1] , and then the subcarrier assignment proceeds on the basis of the maximal SINR criterion.

The initial power distribution $\mathbf{P}_{t_1}$ (t_1 is the index of alternate optimization) can be obtained by allocating little power on each subcarrier, and each SU selects their subcarriers according to:

$$\theta_f^{nm'} = 1, \quad m' = \arg \max_{m=1,2,\ldots,M} \frac{\left(p^{nf}\right)_{t_1} g_{nm}^{nf}}{\sigma^2 + I_{\text{ps}} + I_{\text{ss}}}. \tag{13}$$

After accomplishing subcarrier allocation (i.e., the integer variable is excluded), and the residual problem in **Q1** is reformulated as **Q2**:

$$\max_{p^{nf}} \quad \frac{\sum_{n=1}^{N}\sum_{f=1}^{F} \log_2\left(1 + \frac{p^{nf} g_{nm}^{nf}}{\sigma^2 + I_{\text{ps}} + I_{\text{ss}}}\right)}{\sum_{n=1}^{N}\left(P_{\text{dp}} + P_{\text{sp}} + \sum_{f=1}^{F} \xi p^{nf}\right)} \tag{14}$$

$$\text{s.t.} \begin{cases} \sum_{f=1}^{F} p^{nf} \le P_{\text{th}}, \quad \forall n; & \text{(14a)} \\ 0 \le p^{nf} \le P_{\text{sub}}, \quad \forall n, f; & \text{(14b)} \\ \sum_{f=1}^{F} p^{nf} \widetilde{h}_{\text{sp}}^{nf} V_{\pi(f,l)} \le I_{\text{th}}^{l}, \quad \forall n, l. & \text{(14c)} \end{cases}$$

Once the solution of **Q2** is obtained, the subcarrier assignment will be executed until convergence. The procedures of this alternate optimization are summarized in line 2 ∼ 12 of Algorithm 1.

The convergence property can be derived with the following idea. For a given power allocation $\mathbf{P}_{t_1}$, the maximal SINR criteria maximize the objective within the feasible subcarrier assignment $\boldsymbol{\theta}_{t_1+1}$. And for a fixed $\boldsymbol{\theta}_{t_1}$, $\mathbf{P}_{t_1}$ is the optimal solution of maximizing the objective within the feasible power distribution. In other words, the arbitrary optimization of $\boldsymbol{\theta}$ and $\mathbf{P}$ will improve the objective during the alternate process. Therefore, Algorithm 1 is convergent.

3.2 Power optimization

3.2.1 An equivalent transformation

It is observed that the objective function in **Q2** has a ratio structure consisting of a non-convex function and a linear function, which is known as a fractional programming problem. Generally, the routine method [25, 26, 38] of solving such problem is to transform the objective function into a parametric subtracted form. It needs to update the parameter of the ratio iteratively according to the Dinkelbach algorithm reported in [44] or bisection method [45].

While in this paper, we do not invoke the Dinkelbach procedure to make the subtracted transformation and iteratively update the ratio. Inspired by [39], we solve the problem with the ratio structure by means of a novel equivalent transformation which can directly acquire the optimal value of the ratio. Let us introduce some auxiliary variables x, y, and η. Define the following problem **Q3**:

$$\max_{p^{nf},\eta,x,y} \quad \eta \tag{15}$$

$$\text{s.t.} \begin{cases} \sum_{f=1}^{F} p^{nf} \le P_{\text{th}}, \quad \forall n; & \text{(15a)} \\ 0 \le p^{nf} \le P_{\text{sub}}, \quad \forall n, f; & \text{(15b)} \\ \sum_{f=1}^{F} p^{nf} \widetilde{h}_{\text{sp}}^{nf} V_{\pi(f,l)} \le I_{\text{th}}^{l}, \quad \forall l; & \text{(15c)} \\ \frac{y^2}{x} \ge \eta; & \text{(15d)} \\ \sum_{n=1}^{N}\sum_{f=1}^{F} \log_2\left(1 + \frac{p^{nf} g_{nm}^{nf}}{\sigma^2 + I_{\text{ps}} + I_{\text{ss}}}\right) \ge y^2; & \text{(15e)} \\ \sum_{n=1}^{N}\left(P_{\text{dp}} + P_{\text{sp}} + \sum_{f=1}^{F} \xi p^{nf}\right) \le x. & \text{(15f)} \end{cases}$$

In **Q3**, η is applied to approximate the original ratio, and x and y are used to approximate the denominator and numerator of the objective function in **Q2** respectively. For **Q3**, we have the following theorem.

Theorem: **Q3** *is an equivalent substitute of* **Q2**.

Proof: The equivalency can be proved by contradiction. Assuming that at the optimal point $(x^*, y^*, \eta^*, \mathbf{P}^*)$, the inequality constraints of (14d), (14e), and (14f) do not hold; therefore, there must exist a point $(x^\circ, y^\circ, \eta^\circ, \mathbf{P}^\circ)$ which improves the optimal value, i.e., $\eta^\circ > \eta^*$. And this contradicts the initial assumption. Thus, we can conclude that the inequality constraints of (14d), (14e), and (14f) must be active at the optimality, i.e., all of (14d), (14e), and (14f) must be equality constraints, and it indicates that **Q2** can be substituted by **Q3**. In the subsequent subsection, we mainly concentrate on how to solve the power allocation problem **Q3**. □

3.2.2 Power allocation based on SCA

On the basis of theorem, we can find the solution of **Q3** instead of solving **Q2** with fractional structure. However, it is clear that solving **Q3** directly is still troublesome due to the non-convexity of constraints (15d) and (15e). The constraint (15d) has a relatively simpler structure than (15e), so we firstly show how to deal with (15d).

Note that the left side of (15d) is a quadratic over linear function which is convex if $x \ge 0$. For a given approximated point $\left\{\widetilde{\mathbf{P}}_{t_2}, \widetilde{x}_{t_2}, \widetilde{y}_{t_2}\right\}$, the following inequality holds true:

$$\frac{y^2}{x} \ge 2\frac{\widetilde{y}_{t_2}}{\widetilde{x}_{t_2}} y - \left(\frac{\widetilde{y}_{t_2}}{\widetilde{x}_{t_2}}\right)^2 x. \tag{16}$$

Define $\Omega(x, y) = 2\frac{\widetilde{y}_{t_2}}{\widetilde{x}_{t_2}} y - \left(\frac{\widetilde{y}_{t_2}}{\widetilde{x}_{t_2}}\right)^2 x$, and bring it into (15d). The constraint (15d) can be represented as:

$$\Omega(x, y) \ge \eta, \tag{17}$$

and it can be found that the constraint (17) is convex.

As for (15e) in **Q3**, the case is more complicated than that of (15d). We rewrite the constraint (15e) as:

$$\sum_{n=1}^{N}\sum_{f=1}^{F}\log_2\left(\delta^2+\sum_{n'=1}^{N}p^{n'f}g_{nm}^{n'f}\right)-y^2 -\sum_{n=1}^{N}\sum_{f=1}^{F}\log_2\left(\delta^2+\sum_{n'=1,n'\neq n}^{N}p^{n'f}g_{nm}^{n'f}\right)\geq 0, \tag{18}$$

where σ^2+I_{ps} is simplified as δ^2. The left side of (18) can be seen as the sum of three terms. The term $-y^2$ approximates the capacity which is a concave function of y, and the other two terms originate from the formula of capacity. The expression (18) leads to a non-convex feasible area; thus, the critical situation lies in how to construct a convex set from (18) on the given approximated point $\{\widetilde{\mathbf{P}}_{t_2},\widetilde{x}_{t_2},\widetilde{y}_{t_2}\}$.

Based on the fact that the value of arithmetic mean is greater than or equal to the value of geometric mean, the following inequality holds true:

$$a_1b_1+a_2b_2+\cdots+a_ib_i\geq b_1^{a_1}b_2^{a_2}\ldots b_i^{a_i}, \tag{19}$$

where $b_i>0$, $a_i\geq 0$ and $\sum_i a_i=1$. The inequality in (19) holds with equality if and only if $a_i=\frac{a_ib_i}{\sum_i a_ib_i},\forall i$. For the sake of convenience, denote $\delta^2+\sum_{n'=1}^{N}p^{n'f}g_{nm}^{n'f}$ in (18) as $\phi(\mathbf{P})$. $\phi(\mathbf{P})$ has the form of arithmetic mean shown in the left of (19). Given point $\{\widetilde{\mathbf{P}}_{t_2},\widetilde{x}_{t_2},\widetilde{y}_{t_2}\}$, the geometric mean approximation can be utilized to approximate $\phi(\mathbf{P})$ if taking $\phi(\mathbf{P})$ as the left part of (19). The corresponding approximated inequality (20) is shown at the top of this page, and the right part of (20) is defined as $\widetilde{\phi}(\mathbf{P})$ which is the counterpart of $\phi(\mathbf{P})$.

$$\begin{aligned}&\phi(\mathbf{P})|_{\mathbf{P}=\widetilde{\mathbf{P}}_{t_2}}\geq\\ &\left(\delta^2+\sum_{n'=1}^{N}\left(\widetilde{p}^{n'f}\right)_{t_2}g_{nm}^{n'f}\right)^{\frac{\delta^2}{\delta^2+\sum_{n'=1}^{N}\left(\widetilde{p}^{n'f}\right)_{t_2}g_{nm}^{n'f}}}\prod_{n'=1}^{N}\\ &\left(\frac{p^{n'f}}{\left(\widetilde{p}^{n'f}\right)_{t_2}}\times\left(\delta^2+\sum_{n'=1}^{N}\left(\widetilde{p}^{n'f}\right)_{t_2}g_{nm}^{n'f}\right)\right)^{\frac{\left(\widetilde{p}^{n'f}\right)_{t_2}g_{nm}^{n'f}}{\delta^2+\sum_{n'=1}^{N}\left(\widetilde{p}^{n'f}\right)_{t_2}g_{nm}^{n'f}}}\\ &\triangleq\widetilde{\phi}(\mathbf{P})\end{aligned} \tag{20}$$

On the surface, the manipulation of (20) expresses the linear function of power variable $\phi(\mathbf{P})$ with a multiplicative function of power variable $\widetilde{\phi}(\mathbf{P})$. But essentially, the manipulation constructs a convex set from a non-convex set on the approximated point $\{\widetilde{\mathbf{P}}_{t_2},\widetilde{x}_{t_2},\widetilde{y}_{t_2}\}$. As a consequence, the original constraint (15e) in **Q3** is approximately written as:

$$\sum_{n=1}^{N}\sum_{f=1}^{F}\log_2\left(\widetilde{\phi}\left(\mathbf{P}\right)\right) -\sum_{n=1}^{N}\sum_{f=1}^{F}\log_2\left(\delta^2+\sum_{n'=1,n'\neq n}^{N}p^{n'f}g_{nm}^{n'f}\right)-y^2\geq 0. \tag{21}$$

By introducing a logarithmic manipulation $\mathbf{P}=\exp\left(\mathbf{P}'\right)$ and bringing it into (21), then the final optimization problem after approximation is formulated as **Q4**:

$$\max_{p'^{nf},\eta,x,y}\quad \eta \tag{22}$$

s.t.

$$\begin{cases}\sum_{f=1}^{F}\exp\left(p'^{nf}\right)\leq P_{\mathrm{th}}, \quad \forall n; & \text{(22a)}\\ \exp\left(p'^{nf}\right)\leq P_{\mathrm{sub}}, \quad \forall n,f; & \text{(22b)}\\ \sum_{f=1}^{F}\exp\left(p'^{nf}\right)\widetilde{h}_{\mathrm{sp}}^{nf}V_{\pi(f,l)}\leq I_{\mathrm{th}}^{l}, \quad \forall n,l; & \text{(22c)}\\ \Omega\left(x,y\right)\geq\eta; & \text{(22d)}\\ \sum_{n=1}^{N}\sum_{f=1}^{F}\log_2\left(\widetilde{\phi}\left(\exp\left(\mathbf{P}'\right)\right)\right) -\sum_{n=1}^{N}\sum_{f=1}^{F}\log_2\left(\psi\left(\exp\left(\mathbf{P}'\right)\right)\right)-y^2\geq 0; & \text{(22e)}\\ \sum_{n=1}^{N}\left(P_{\mathrm{dp}}+P_{\mathrm{sp}}+\sum_{f=1}^{F}\xi\exp\left(p'^{nf}\right)\right)\leq x, & \text{(22f)}\end{cases}$$

where $\psi\left(\exp\left(\mathbf{P}'\right)\right)\triangleq\delta^2+\sum_{n'\neq n,n'\in\mathcal{N}}^{N}\exp\left(p'^{n'f}\right)g_{nm}^{n'f}$.

For the above problem in **Q4**, we have the following two propositions.

Proposition 1 *Q4 is a convex optimization problem.*

Proof Firstly, the sum of exponential functions is convex, so the constraints (22a) ∼ (22c) and (22f) are all convex sets. The constraint (22d) is a linear constraint which is also convex. Lastly, $\sum_{n=1}^{N}\sum_{f=1}^{F}\log_2\left(\widetilde{\phi}\left(\exp\left(\mathbf{P}'\right)\right)\right)$ is a linear function of $\mathbf{P}'$, and it has been proved that the log-sum-exp function is convex [46], so we can find that the left side of (22e) in **Q4** is the sum of linear functions and two concave functions, which implies (22e) is also a convex set. Therefore, the convexity of the constraint sets is verified, i.e., **Q4** is a convex problem. □

The problem **Q4** can be efficiently solved by the existing convex optimization algorithms [46], or the optimization toolbox CVX [47]. However, the solution of **Q4** subject to

constraints only corresponds to initial approximate point $\left\{\widetilde{\mathbf{P}}_{t_2}, \widetilde{x}_{t_2}, \widetilde{y}_{t_2}\right\}$. In order to produce an improvement point compared to $\left\{\widetilde{\mathbf{P}}_{t_2}, \widetilde{x}_{t_2}, \widetilde{y}_{t_2}\right\}$, herein, the SCA in [48, 49] for constraints is employed. Once we obtain the solution of **Q4**, it will take the place of the previous approximated point according to (16) and (20), and the iteration procedure goes on until convergence. The iterative procedure is summarized in line 4 ∼ 10 of Algorithm 1.

Proposition 2 *Each iteration of SCA makes an improvement compared to the previous iteration and the iteration procedure is convergent.*

Proof It is assumed that the optimal solution obtained at the iteration t_2 is $\left\{\mathbf{P}^*_{t_2}, y^*_{t_2}, x^*_{t_2}\right\}$, which is also feasible and satisfies the constraints of Q3 for the next approximation. This mainly results from the fact that the approximated parts of the constraints (22d) and (22e) are less than the original corresponding parts of constraints (15d) and (15e). It indicates that the iteration sequences of the objective are non-decreasing. In addition, the constraints are bounded. Therefore, the process of successive convex approximation finally converges, which proves Proposition 2. □

Moreover, in order to make the iterative sequences stop at or converge to Karush-Kuhn-Tucker (KKT) point, the following conditions are needed for the successive convex approximation [48]:

$$\begin{cases} \Pi(\alpha) \geq \widetilde{\Pi}(\alpha) \\ \Pi(\alpha)\left|_{\alpha=\widetilde{\alpha}} = \widetilde{\Pi}(\alpha)\right|_{\alpha=\widetilde{\alpha}} \\ \nabla\Pi(\alpha)\left|_{\alpha=\widetilde{\alpha}} = \nabla\widetilde{\Pi}(\alpha)\right|_{\alpha=\widetilde{\alpha}} \end{cases} \tag{23}$$

where Π is a function of variable α.

It can be verified that the approximation of (16) and (20) satisfies the above three conditions. In (23), the first condition guarantees the approximation is tightening the constraints of (15d) and (15e), and the solution of approximated problem is also a feasible point for the next approximation; the second condition ensures the improvement of the objective during each iteration; the last condition ensures the satisfaction of the KKT conditions after a series of iteration approximation.

4 Complexity analysis

In this section, the computational complexity of the proposed algorithm is analyzed. The optimization toolbox CVX is applied to solve **Q4** via the interior point method (IPM), which dominates the main complexity of the whole algorithm. In IPM, by contaminating the objective and inequality constraints, a logarithmic barrier function is constructed and optimized along a central path through Newton method. With self-concordance for this function, the number of Newton steps is proportional to the square root of the number of inequality constraints, and the complexity of each Newton increases cubically with the number of inequality constraints [46, 50].

The analogous means of [50] can be adopted to transform the constraints with log-sum-exp into a set of equivalent constraints with self-concordance. The total number of equivalent constraints is $6FN + N + 2FLN + L + 2FN^2$. Therefore, the whole complexity is $\mathcal{O}\left(T_1 T_2 \left(FLN + FN^2\right)^{3.5}\right)$ after eliminating the multiplicative factors and non-dominant terms, where T_1 and T_2 are the numbers of alternate optimization and successive convex approximation, respectively.

5 Simulation results and discussions

In this section, numerical results of the proposed RA algorithm by Monte Carlo are conducted and compared with two algorithms [19, 23]. Moreover, the impacts of different 5G waveforms and system dimensions are also simulated and analyzed. To be more specific, the simulation results are divided into three parts: The first part presents the efficiency including the convergence and the performance comparison between the proposed algorithm and the two existing algorithms in [19, 23]; the second part exhibits the performance of four potential 5G waveforms in terms of different parameter settings; and the last part evaluates the impact of different system dimensions on the energy efficiency. The simulation parameters are presented in Table 2, and the ones which are changed will be declared.

Considering the CR-enabled 5G system shown in Fig. 1, where the PBS lies in the center of the primary system, the PUs are randomly located around the PBS within the cell range. We firstly investigate the efficiency of the proposed algorithm. The convergence of alternate optimization and SCA is shown in Figs. 3 and 4. According to the convergence behavior in Fig. 3, we can find that the alternate optimization of subcarrier assignment and power allocation converges after several operations. It is interesting to note that no matter what initial power allocation is given for the subcarrier assignment, the results converge to the same solution even if an infeasible power allocation

Table 2 Simulation parameters

Parameters	Value
Cell range	0.1∼2 km
Total subcarrier, F_{tot}	12
Number of cells, N	4
Number of users, M	3
Number of available subcarrier, F	8
Inverse of drain efficiency, ξ	5
P_{dp}	3.1 W
P_{sp}	1.9 W
Pathloss (dB)	128.1+37.6log10(d)
Bandwidth	15 KHz
σ^2	− 174 dBm/Hz

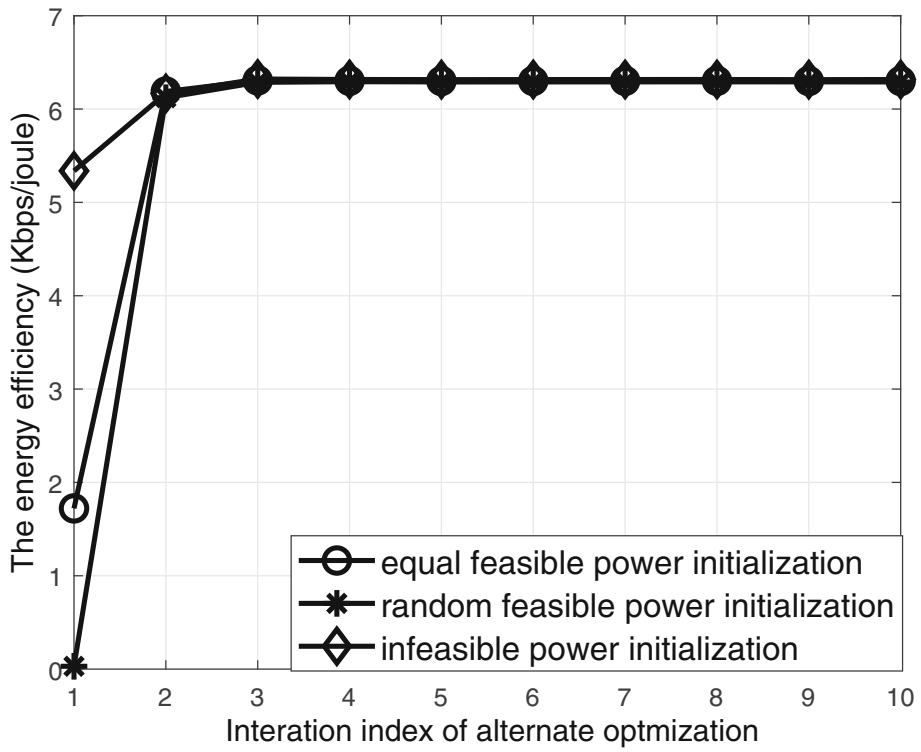

Fig. 3 The convergence of alternate optimization. Convergence behavior of alternate optimization with different initial power allocation

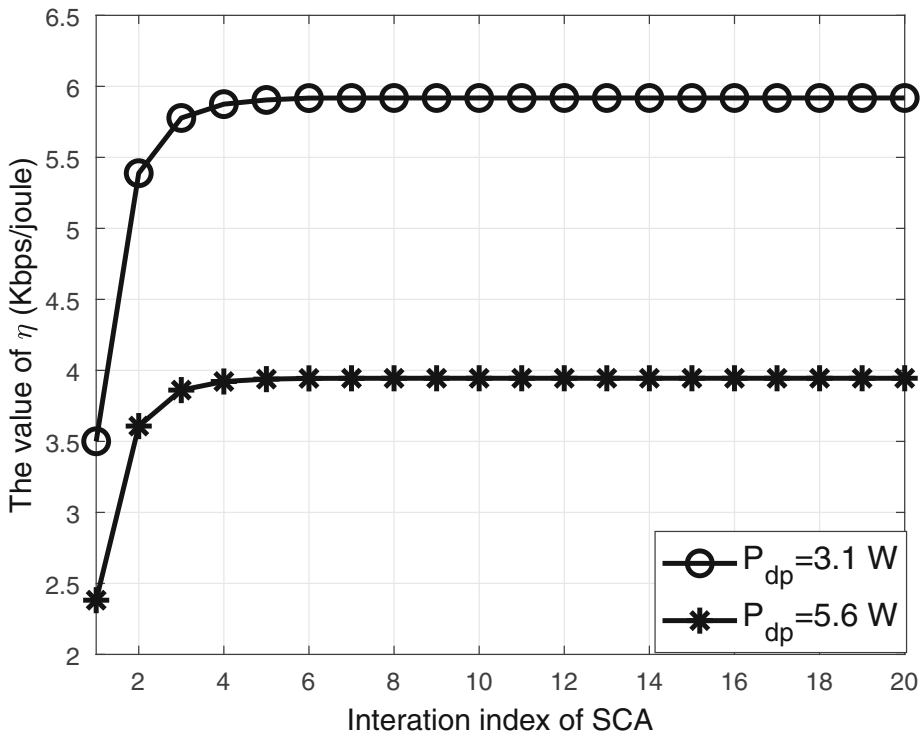

Fig. 4 The convergence of SCA. Convergence behavior of SCA under different P_{dp}

is initialized. This is because it can introduce a feasible power allocation for the subcarrier assignment induced by the infeasible initial power allocation. Figure 4 exhibits the convergence of SCA given the subcarrier assignment. The procedure of successive convex approximation of updating η converges within 10 iterations. Thus, the practical applicability of SCA can be verified.

Besides, in order to illustrate the superiority, the proposed algorithm is compared with two algorithms, i.e., IILA in [19] and DPGA in [23], as shown in Fig. 5. For the sake of fairness, all algorithms are compared on the basis of energy efficiency. Here, we only consider the case of FBMC in Table 1. The capacity guarantee coefficient β associated with the level of interference threshold is set to 0.8. As the sum power budget augments, it is seen that all of the curves in Fig. 5 firstly increase and then slowly approach a constant. It can be explained that the numerator in (8) has a logarithmic structure with power variable, while the power consumption in the denominator is linear. The value of energy efficiency initially increases because the incremental portion of capacity plays the dominant role relative to the increment of power consumption, and the energy efficiency finally remains constant because the opposite situation follows. Therefore, a turning point must exist in line with the point firstly approaching the constant. For the proposed algorithm, the turning point is achieved at 16 dBm.

In Fig. 5, we also observe that the proposed algorithm achieves higher energy efficiency in both cases of either low-power budget or high-power budget. With the same power consumption, the proposed algorithm has the largest capacity, i.e., our algorithm needs the least consumption to achieve the same capacity. The reason is that a linear pricing factor is required to impose the penalty for the DPGA in [23], which is avoided in the proposed algorithm. For IILA in [19], the co-channel interference is assumed to be constant, while the proposed algorithm makes an improvement for the co-channel interference by using the successive convex approximation.

In the second parts of the experiments, the impacts of the proposed algorithm with different system parameters on energy efficiency by using various 5G waveforms are presented. The first three figures are obtained under ideal channel gain, and the last one is obtained under estimated channel gain.

Figure 6 shows the relation between the energy efficiency of waveforms with power budget of each cell. It is seen that all curves have the same tendency and almost the same turning point. The difference among these waveforms is that these waveforms have different levels of spectral leakage. The case of PS provides a theoretic upper bound and is viewed as the benchmark because the spectral leakage is not involved. Note that FBMC achieves the highest energy efficiency and is the closest to the case

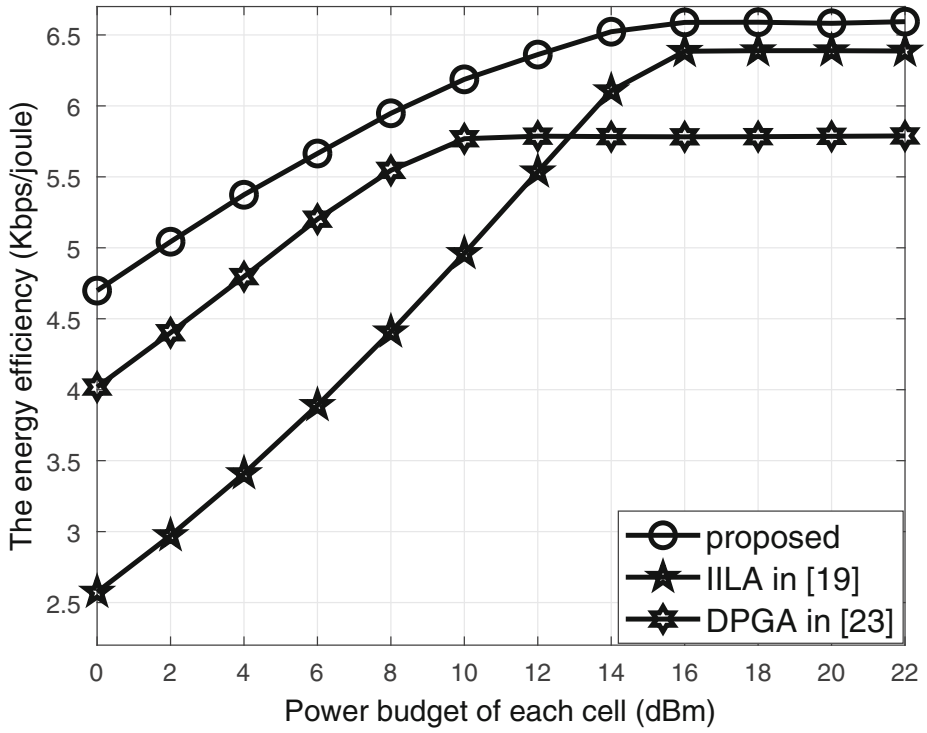

Fig. 5 Comparison of algorithms. The performance comparison of the proposed algorithm with some existing ones versus different sum power budgets

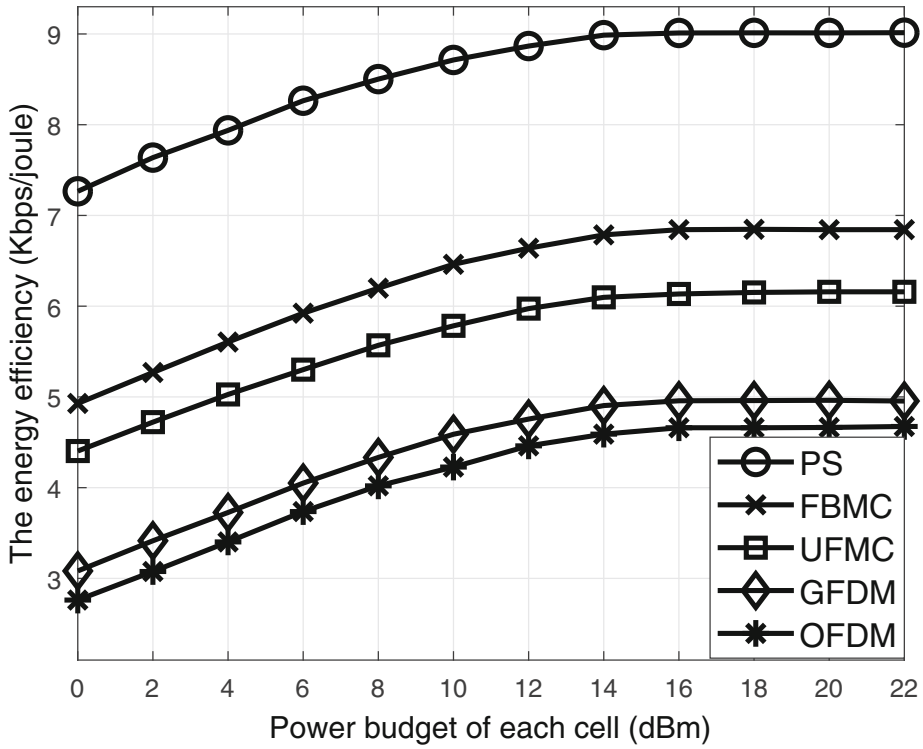

Fig. 6 Energy efficiency versus power budget. The performance of the proposed algorithm using various modulation schemes versus different sum power budgets

of PS, while OFDM has the worst performance among all the waveforms due to its significant spectral leakage. Although the first element of GFDM in Table 1 is less than that of FBMC, the remaining elements of GFDM are larger than those of FBMC, which explains the worse performance of GFDM than FBMC. At last, FBMC and UFMC have similar performance due to their similar interference vectors. As a conclusion, the less the spectral leakage is, the higher energy efficiency can be achieved.

Figure 7 displays the relation between the energy efficiency of waveforms with power limits on each subcarrier. The power budget of each cell is set to 16 dBm. The energy efficiency firstly increases and then maintains a constant when the power limit increases from 1 to 10 mW. In Fig. 7, we can see that the most appropriate power limit of subcarrier is about 6 mW, where the value of energy efficiency firstly approaches the maximum. The reason is that the large power limit of subcarriers enlarges the capacity until the energy efficiency achieves the maximum, and subsequently, the other constraints restrict the growing of capacity.

We also investigate the impacts of different waveforms under different interference thresholds, as shown in Fig. 8, where the maximal power consumption of each cell and power limit of each subcarrier are 16 dBm and 5 mW, respectively. Except for the PS case (interference to PU does not exist), all other curves increase as the value of $1-\beta$ augments. If a large interference threshold from secondary cells to PUs is permitted, the SBS will transmit more power to its corresponding SUs. This explains the rise of the curves in Fig. 8 when the interference threshold increases. In addition, the same conclusion as in Fig. 6 is made, i.e., FBMC has the highest energy efficiency under the same interference threshold.

The impact of estimated channel gain is depicted in Fig. 9. Since the case of PS does not introduce interference due to spectral leakage, the constraint (10) loses efficacy, which induces the horizontal curve of PS (like the case in Fig. 8). As the outage probability increases uniformly, the estimated margin decreases rapidly firstly and then decreases slowly. It implies that the transmission power can enlarge rapidly first which induces significant co-channel interference and power consumption, thus the energy efficiency declines, and subsequently, the transmission power increases slowly, the co-channel interference and power consumption strengthen slowly too, which results in the rising tendency of energy efficiency.

In the last part of the experiments, the impacts of two important parameters about system dimensions on energy efficiency are shown in Figs. 10 and 11, where we consider the influence of the number of secondary cells and the number of SUs per cell respectively, and FBMC is

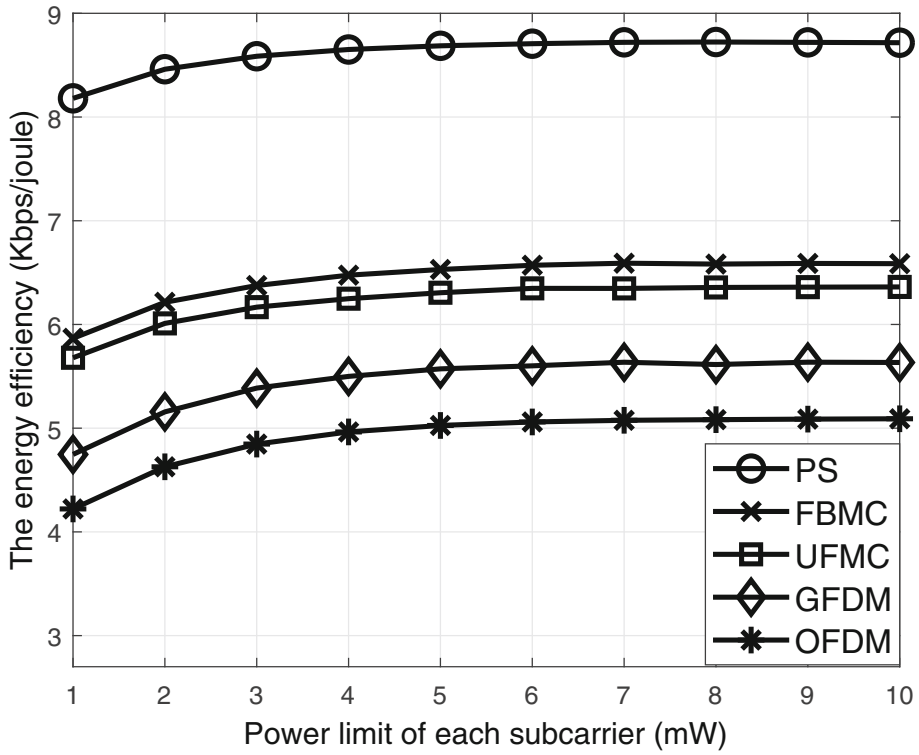

Fig. 7 Energy efficiency versus power limits. The performance of the proposed algorithm using various modulation schemes versus different power limits on subcarriers

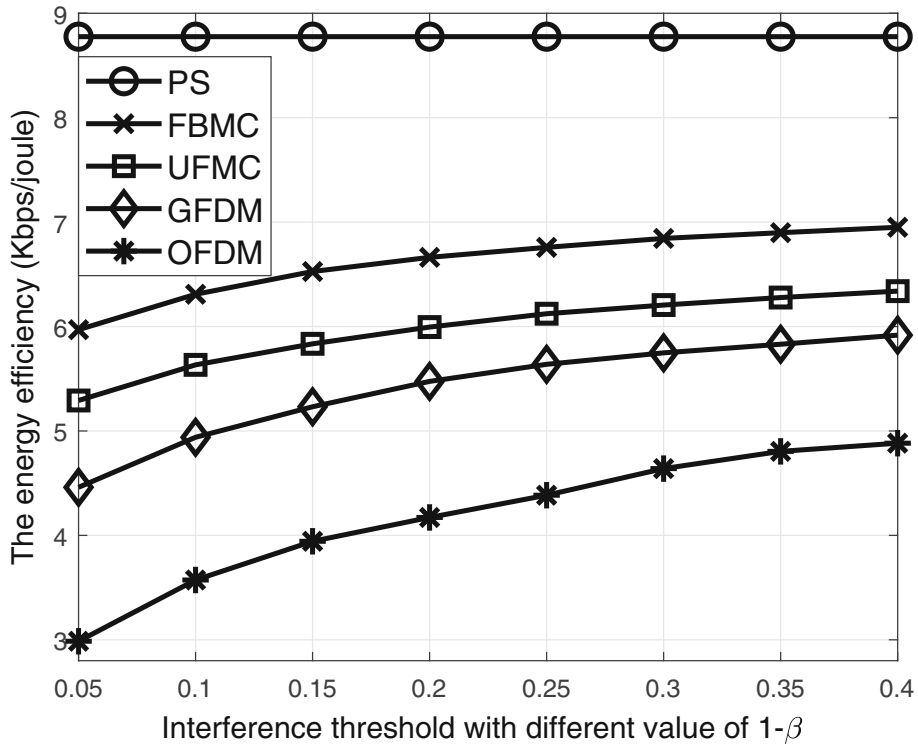

Fig. 8 Energy efficiency versus interference thresholds. The performance of the proposed algorithm using various modulation schemes versus different interference thresholds

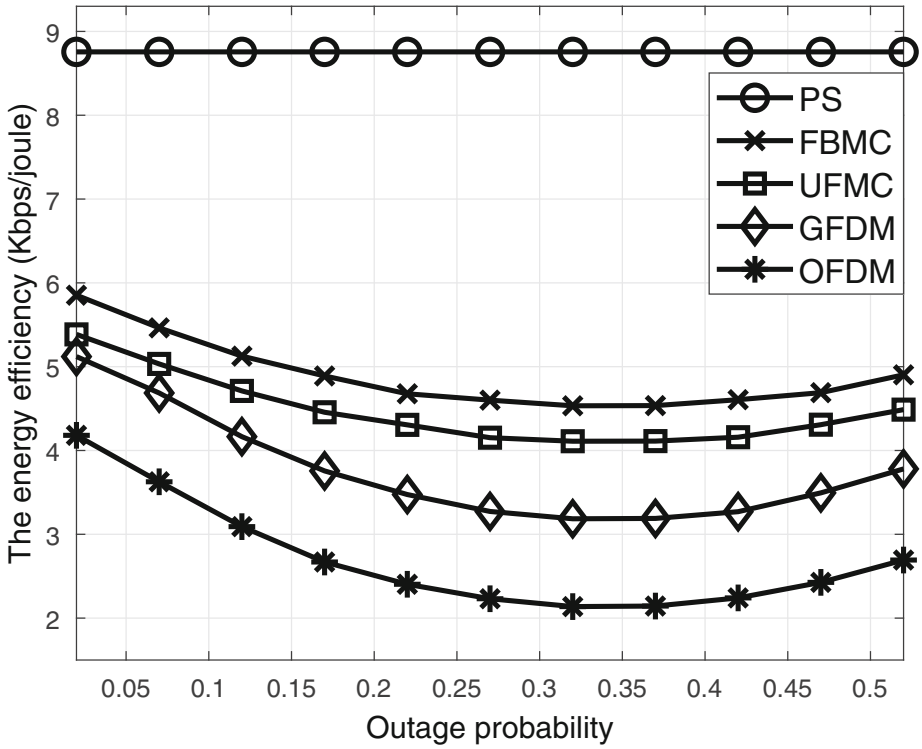

Fig. 9 Energy efficiency versus outage probability. The performance of the proposed algorithm using various modulation schemes versus different outage probability

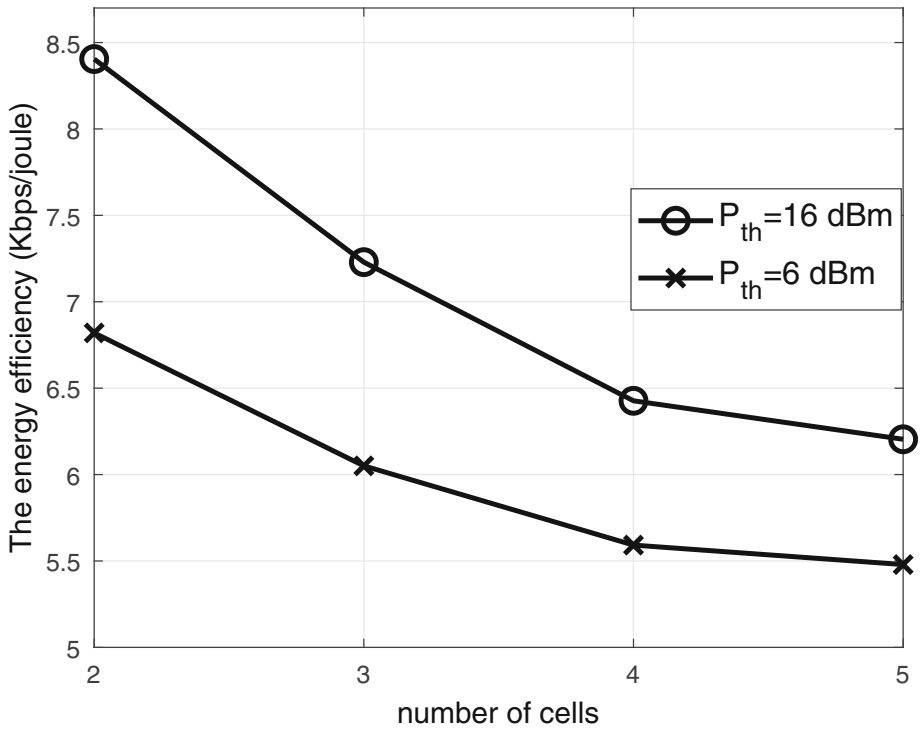

Fig. 10 Energy efficiency versus number of secondary cells. The performance of the proposed algorithm with different number of secondary cells

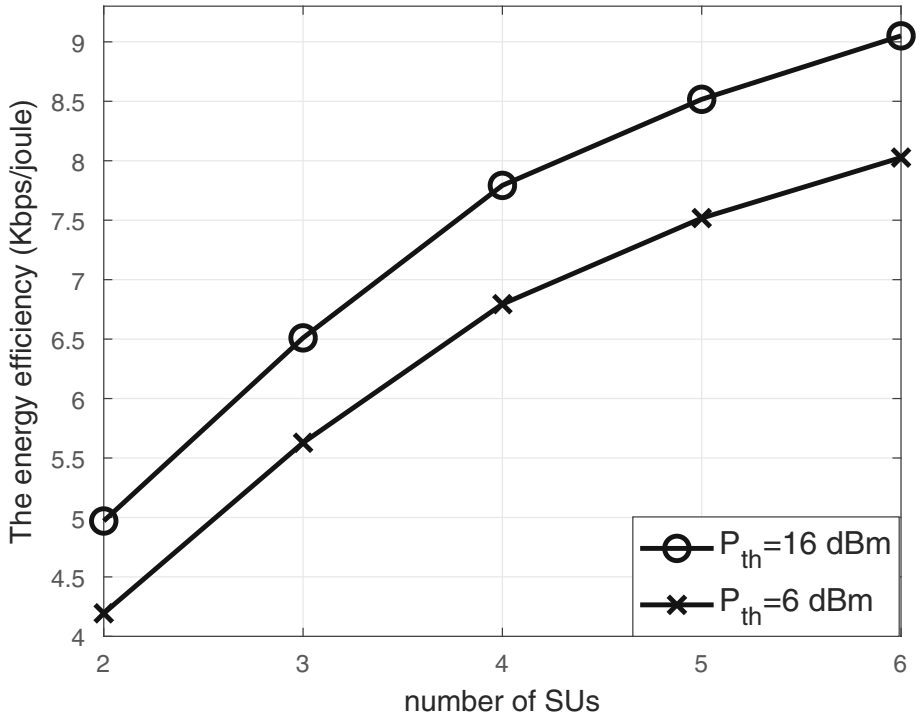

Fig. 11 Energy efficiency versus number of SUs. The performance of the proposed algorithm with different number of SUs per cell

selected as the waveform. In Fig. 10, the number of SUs is fixed to 3, and the number of secondary cells is set to 2, 3, 4, and 5. Observe that the number of cells has a negative effect on the system performance, i.e., an energy-efficient system should pay attention to the number of cells. Because a large-cell structure will inevitably generate significant co-channel interference among cells and result in the capacity degradation for each cell, although the whole system capacity increases. From the perspective of spectral efficiency, the more the number of cells is, the higher the capacity is. When the energy efficiency is concerned, the increasing number of cells will cause lower energy efficiency. Consequently, we need to make a trade-off between energy efficiency and spectral efficiency if the future 5G system considers a large number of cognitive cells.

In Fig. 11, the number of cells is fixed to 3, and the number of SUs is set to 2, 3, 4, 5, and 6. According to Fig. 11, it can be found that the number of the SUs will bring higher energy efficiency. This results from the fact that the increasing number of the SUs enlarges the system capacity when the system power budget remains constant, i.e., the ratio of capacity to consumption is increased. Therefore, more SUs benefit the energy efficiency performance. However, we also can forecast that under the conditions of given number of subcarriers, more SUs means less accessing opportunity and worse quality of service (QoS). The trade-off of the system energy efficiency and the QoS of SUs also need to be considered.

6 Conclusions

This paper proposes an energy-efficient resource allocation algorithm aiming at solving the awkward non-convex problem involving multiple cells with multiple SUs per cell. The heuristic subcarrier assignment and convex approximation are adopted to sequentially transform the non-convex form into a convex one. Numerical results validate the superiority of the proposed algorithm for achieving higher energy efficiency compared with some existing algorithms. Furthermore, the impacts of potential modulation schemes in 5G on energy efficiency are also investigated, and we reach the conclusion that the waveform with less spectral leakage is more suitable for energy-efficient 5G systems.

Endnote

[1] Generally, it makes no difference whether the initial power is feasible or not, which will be demonstrated by the subsequent simulation.

Acknowledgements

This work was supported by the National Natural Science Foundation of China with Grant Number 61501335 and Hubei Provincial Natural Science Foundation of China (No. 2018CFB225).

Funding
National Natural Science Foundation of China with Grant Number 61501335 and Hubei Provincial Natural Science Foundation of China (No. 2018CFB225).

Availability of data and materials
Not applicable.

Authors' contributions
HL and PL conceived and designed the study. HZ performed the experiments. HL wrote the paper. PL, HZ, and QY reviewed and edited the manuscript. All authors read and approved the manuscript.

Ethics approval and consent to participate
Not applicable.

Consent for publication
Not applicable.

Competing interests
The authors declare that they have no competing interests.

Publisher's Note

Received: 31 May 2018 Accepted: 20 December 2018
Published online: 18 January 2019

References

1. Q. Wu, G. Y. Li, W. Chen, D. W. K. Ng, R. Schober, An overview of sustainable green 5G networks. IWirel. EEE. Commun. **24**(4), 72–80 (2017)
2. S. Zhang, Q. Wu, S. Xu, G. Y. Li, Fundamental green tradeoffs: progresses, challenges, and impacts on 5G networks. ICommun, EEE, Surv. Tutor. **19**(1), 33–56 (2017)
3. M. Agiwal, A. Roy, N. Saxena, Next generation 5G wireless networks: a comprehensive survey. ICommun. EEE. Surv. Tutor. **18**(3), 1617–1655 (2016)
4. R. H. Tehrani, S. Vahid, D. Triantafyllopoulou, H. Lee, K. Moessner, Licensed spectrum sharing schemes for mobile operators: a survey and outlook. ICommun. EEE. Surv. Tutor. **18**(4), 2591–2623 (2016)
5. P. Kolodzy, Spectrum policy task force report. Federal Commun. Comm. Washington DC Rep. Docket ET. **40**(4), 147–158 (2002)
6. H. Mu, T. Hu, *Cognitive radio and the new spectrum paradigm for 5G*. (M. A. Matin, ed.) (Springer, Singapore, 2017), pp. 265–286
7. X. Hong, J. Wang, C. X. Wang, J. Shi, Cognitive radio in 5G: a perspective on energy-spectral efficiency trade-off. ICommun. EEE Mag. **52**(7), 46–53 (2014)
8. L. Zhang, M. Xiao, G. Wu, M. Alam, Y. C. Liang, S. Li, A survey of advanced techniques for spectrum sharing in 5G networks. ICommun. EEE Mag. **24**(5), 44–51 (2017)
9. A. Georgakopoulos, A. Margaris, K. Tsagkaris, P. Demestichas, Resource sharing in 5G contexts: achieving sustainability with energy and resource efficiency. IVeh EEE Technol. Mag. **11**(1), 40–49 (2016)
10. Y. Huang, M. Liu, Y. Liu, Energy-efficient SWIPT in IoT distributed antenna systems. IEEE J. Internet Things. **5**(4), 2646–56 (2018)
11. J. Yan, Y. Liu, A dynamic SWIPT approach for cooperative cognitive radio networks. ITrans EEE Veh. Technol. **66**(12), 11122–11136 (2017)
12. M. Shaat, F. Bader, Computationally efficient power allocation algorithm in multicarrier-based cognitive radio networks: OFDM and FBMC systems. EURASIP J. Adv. Signal Process. **2010**(1), 1–13 (2010)
13. S. Dikmese, S. Srinivasan, M. Shaat, F. Bader, M. Renfors, Spectrum sensing and resource allocation for multicarrier cognitive radio systems under interference and power constraints. EURASIP J. Adv. Signal Process. **2014**(1), 1–12 (2014)
14. S. Wang, Z. H. Zhou, M. Ge, C. Wang, Resource allocation for heterogeneous cognitive radio networks with imperfect spectrum sensing. IEEE J. Sel. Areas Commun. **31**(3), 464–475 (2013)
15. T. Abrão, S. Yang, L. D. H. Sampaio, P. J. E. Jeszensky, L. Hanzo, Achieving maximum effective capacity in OFDMA networks operating under statistical delay guarantee. IAccess, EEE,. **5**, 14333–14346 (2017)
16. S. Wang, W. Shi, C. Wang, Energy-efficient resource management in OFDM-based cognitive radio networks under channel uncertainty. ITrans EEE Commun. **63**(9), 3092–3102 (2015)
17. H. Zhang, D. L. Ruyet, D. Roviras, Y. Medjahdi, H. Sun, Spectral efficiency comparison of OFDM/FBMC for uplink cognitive radio networks. EURASIP J. Adv. Signal Process. **2010**(1), 1–14 (2010)
18. Z. Hu, Y. Zhu, J. Xu, J. Wang, Y. Yang, Distributed weighted sum-rate maximization with multi-cell uplink-downlink throughput duality. EURASIP J. Adv. Signal Process. **2015**(1), 31–46 (2015)
19. H. Zhang, C. Jiang, X. Mao, H. H. Chen, Interference-limited resource optimization in cognitive femtocells with fairness and imperfect spectrum sensing. ITrans EEE Veh. Technol. **65**(3), 1761–1771 (2016)
20. H. Zhang, D. L. Ruyet, D. Roviras, H. Sun, Noncooperative multicell resource allocation of FBMC-based cognitive radio systems. ITrans EEE Veh. Technol. **61**(2), 799–811 (2012)
21. H. Lv, P. Li, H. Zhang, Y. Qian, in *2016 IEEE 13th International Conference on Signal Processing (ICSP)*. Resource allocation in FBMC-based two-cell cognitive radio systems with estimated CSI, (2016), pp. 1301–1306
22. W. Jing, Z. Lu, X. Wen, Z. Hu, S. Yang, Flexible resource allocation for joint optimization of energy and spectral efficiency in OFDMA multi-cell networks. ICommun EEE Lett. **19**(3), 451–454 (2015)
23. S. Bu, F. R. Yu, in *2014 IGlobal, EEE, Communications Conference*. Distributed energy-efficient resource allocation with fairness in wireless multicell OFDMA networks, (2014), pp. 4708–4713
24. A. Zappone, L. Sanguinetti, M. Debbah, Energy-delay efficient power control in wireless networks. ITrans. EEE. Commun. **66**(1), 418–431 (2018)
25. K. Yang, S. Martin, D. Quadri, J. Wu, G. Feng, Energy-efficient downlink resource allocation in heterogeneous OFDMA networks. ITrans. EEE. Veh. Technol. **66**(6), 5086–5098 (2017)
26. Z. Tong, B. Li, Y. Hui, Energy efficiency maximisation in downlink multi-cell networks via coordinated resource allocation. Commun. IET,. **9**(1), 42–54 (2015)
27. Y. Medjahdi, M. Terré, D. L. Ruyet, D. Roviras, J. A. Nossek, L. Baltar, in *2009 IEEE 10th Workshop on Signal Processing Advances in Wireless Communications*. Inter-cell interference analysis for OFDM/FBMC systems, (2009), pp. 598–602
28. Y. Medjahdi, M. Terré, D. L. Ruyet, D. Roviras, A. Dziri, Performance analysis in the downlink of asynchronous OFDM/FBMC based multi-cellular networks. ITrans. EEE. Wirel. Commun. **10**(8), 2630–2639 (2011)
29. Y. Medjahdi, M. Terré, D. Le Ruyet, D. Roviras, Interference tables: a useful model for interference analysis in asynchronous multicarrier transmission. EURASIP J. Adv. Signal Process. **2014**(1), 1–17 (2014)
30. H. Zhang, H. Lv, P. Li, in *Towards 5G wireless networks - a physical layer perspective*, ed. by H. K. Bizaki. Spectral efficiency analysis of filter bank multi-carrier (FBMC) based 5G networks with estimated channel state information (CSI) (InTech, Rijeka, 2016)
31. Y. Liu, X. Chen, Z. Zhong, B. Ai, D. Miao, Z. Zhao, J. Sun, Y. Teng, H. Guan, Waveform design for 5G networks: analysis and comparison. IAccess. EEE. **5**, 19282–19292 (2017)
32. Y. Cai, Z. Qin, F. Cui, G. Y. Li, J. A. McCann, Modulation and multiple access for 5G networks. ICommun. EEE. Surv. Tutor. **PP**(99), 1–1 (2017)
33. C. Kim, Y. H. Yun, K. Kim, J. Y. Seol, Introduction to QAM-FBMC: from waveform optimization to system design. ICommun. EEE, Mag. **54**(11), 66–73 (2016)
34. J. Z. Jiang, B. W. K. Ling, S. Ouyang, Efficient design of prototype filter for large scale filter bank-based multicarrier systems. Signal IET Proc. **11**(5), 521–526 (2017)
35. Y. Medjahdi, S. Traverso, R. Gerzaguet, H. Shaïek, R. Zayani, D. Demmer, R. Zakaria, J. B. Doré, M. B. Mabrouk, D. L. Ruyet, Y. Louët, D. Roviras, On the road to 5G: comparative study of physical layer in mtc context. IAccess EEE. **5**, 26556–26581 (2017)
36. B. Lim, Y. C. Ko, SIR analysis of OFDM and GFDM waveforms with timing offset, CFO, and phase noise. ITrans. EEE. Wirel. Commun. **16**(10), 6979–6990 (2017)
37. L. Zhang, P. Xiao, A. Quddus, Cyclic prefix-based universal filtered multicarrier system and performance analysis. ISignal. EEE. Process. Lett. **23**(9), 1197–1201 (2016)
38. J. Denis, M. Pischella, D. L. Ruyet, Energy-efficiency-based resource allocation framework for cognitive radio networks with FBMC/OFDM. ITrans. EEE. Veh. Technol. **66**(6), 4997–5013 (2017)

39. K. G. Nguyen, L. N. Tran, O. Tervo, Q. D. Vu, M. Juntti, Achieving energy efficiency fairness in multicell MISO downlink. ICommun. EEE. Lett. **19**(8), 1426–1429 (2015)
40. K. G. Nguyen, Q. D. Vu, M. Juntti, L. N. Tran, Distributed solutions for energy efficiency fairness in multicell MISO downlink. ITrans. EEE. Wirel. Commun. **16**(9), 6232–6247 (2017)
41. J. Wang, W. Feng, Y. Chen, S. Zhou, Energy efficient power allocation for multicell distributed antenna systems. ICommun. EEE. Lett. **20**(1), 177–180 (2016)
42. W. Feng, Y. Chen, N. Ge, J. Lu, Optimal energy-efficient power allocation for distributed antenna systems with imperfect CSI. ITrans. EEE. Veh. Technol. **65**(9), 7759–7763 (2016)
43. C. Zhong, C. Li, L. Yang, Z. He, in *2008 International Conference on Neural Networks and Signal Processing*. Dynamic resource allocation for the downlink of multi-cell systems with full spectral reuse, (2008), pp. 173–177
44. W. Dinkelbach, On nonlinear fractional programming. Manag. Sci. **13**(7), 492–498 (2011)
45. Y. Chen, Z. Zheng, Y. Li, Y. Li, Energy-efficient resource allocation in multiuser OFDM systems with proportional rate constraints. Electron. Lett. **51**(20), 1611–1613 (2015)
46. S. Boyd, L. Vandenberghe, *Convex optimization*. (Cambridge University Press, Cambridge, 2004)
47. M. Grant, S. Boyd, *CVX: Matlab Software for disciplined convex programming, version 2.1*, (2014). http://cvxr.com/cvx
48. M. Chiang, C. W. Tan, D. P. Palomar, D. O'neill, D. Julian, Power control by geometric programming. ITrans. EEE. Wirel. Commun. **6**(7), 2640–2651 (2007)
49. A. Zappone, L. Sanguinetti, G. Bacci, E. Jorswieck, M. Debbah, Energy-efficient power control: a look at 5G wireless technologies. ITrans. EEE. Signal Process. **64**(7), 1668–1683 (2016)
50. R. Rashtchi, R. H. Gohary, H. Yanikomeroglu, Generalized cross-layer designs for generic half-duplex multicarrier wireless networks with frequency-reuse. ITrans. EEE. Wirel. Commun. **15**(1), 458–471 (2016)